Received: 13 August 2023 | Revised: 10 December 2023 | Accepted: 13 December 2023
DOI: 10.1002/pat.6280

SHORT COMMUNICATION

polymers for advanced technologies WILEY

Development of an intuitive visualization system for measuring the melt electrowritten (MEW) jet diameter along the spinline

Zhiguang Zhou[1] | Ke Lu[2] | Haoxuan Wang[2] | Sherry Ashour[3] | Hangyue Chen[1] | Huaizhong Xu[3] | Ting Xu[4]

[1]School of Media and Design, Hangzhou Dianzi University, Hangzhou, China
[2]School of Computer Science, Hangzhou Dianzi University, Hangzhou, China
[3]Department of Biobased Materials Science, Kyoto Institute of Technology, Kyoto, Japan
[4]Department of Stomatology, First Affiliated Hospital, Zhejiang University, Hangzhou, China

Correspondence
Huaizhong Xu, Department of Biobased Materials Science, Kyoto Institute of Technology, Kyoto, 606-8585, Japan.
Email: xhz2008@kit.ac.jp

Ting Xu, Department of Stomatology, First Affiliated Hospital, Zhejiang University, Hangzhou, 310018, China.
Email: xut@zju.edu.cn

Funding information
Public Welfare Plan Research Project of Zhejiang Provincial Science and Technology Department, Grant/Award Number: LTGG23H260003; National Natural Science Foundation of China, Grant/Award Numbers: 62177040, 62277013; National Statistical Science Research Project, Grant/Award Number: 2023LZ035

Abstract
Melt electrowriting (MEW) is a young and promising additive manufacturing technology for producing high-precision scaffolds. In this study, we develop an intuitive visualization system enabling users to measure MEW jet diameters along the spinline without programming knowledge. The digital measurement adopts the same theory as our reported manual measurement. The maximum error between the digitally and manually measured data is smaller than 9%, suggesting that the open-source system developed here is reliable in measuring jet diameters.

KEYWORDS
3D printing, electrohydrodynamics, electrospinning, jet diameter, software

1 | INTRODUCTION

Melt electrowriting (MEW) is an advanced additive manufacturing technology for printing high-resolution tissue engineering scaffolds.[1] With over one decade of development, numerous MEW-related devices have been established. For instance, researchers developed MEW devices that can print large-scale scaffolds,[2] tubes,[3] core-sheath filaments,[4] and so forth. Meanwhile, the phenomena of jet lag,[5] jet pulsing,[6] fiber bridging,[7] and layer shifting[8] were investigated, highlighting the viewpoint that jet control greatly influences print quality.[9]

Currently, the jet lag angle[10] and the area of Taylor cone[11] are regarded as crucial indexes to judge the stability of printing throughout. Researchers can easily record jet lag angle and Taylor cone. In addition, jet diameter along the spinline is another critical parameter relating to the jet's kinematics and dynamics. We captured clear photos of the moving jet and manually measured the jet diameter along the spinline.[12] According to the mass conservation equation, we can estimate the jet velocities from the jet diameters. However, the current data processing method is time-consuming, and the results vary with each individual. In this context, we develop a web-based application to process the original image of the MEW jet and automatically output the jet diameter. Thus, it is convenient for MEW-related researchers to achieve the essential data without any programming knowledge.

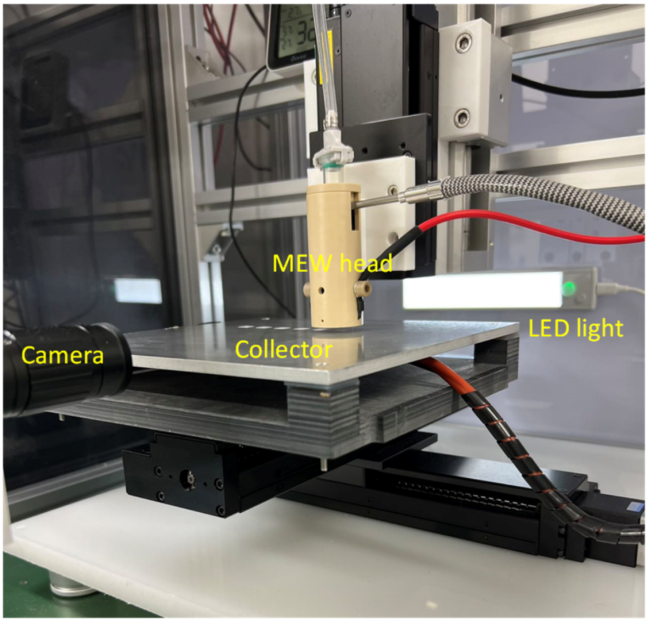

FIGURE 1 The updated vision system of the Melt electrowriting printer.

2 | EXPERIMENTAL

2.1 | Updated vision system

Figure 1 shows an updated vision system within a self-built MEW printer that was reported previously.[13] The primary change is the light source. We adopt an LED light (Brand: Yeezen) with changeable intensity. The light is fixed behind the print head. A 300× lens equipped camera (XW200, Shenzhen Hayear Electronics Co., Ltd., China) is fixed in front of the print head. Notably, the camera, nozzle, and a light source should be placed in the same horizontal line.

2.2 | Printing

Medical-grade polycaprolactone (PCL) with an inherent viscosity of 1.0 ~ 1.3 dL/g (Purasorb, PC12) is used for MEW. The fixed printing parameters are 22 G nozzle, 4 kV applied voltage, 3 mm nozzle-to-collector distance, 100 kPa air pressure, and 73°C heating temperature. Under this condition, the critical translation speed (CTS) is 0.9 mm/s. The CTS is a translation speed that equals the jet speed at the end of the spinline, and the jet is perpendicular to the collector at CTS. The jet lags behind the print direction when the translation speed is higher than the CTS, drawing a straight line on the collector. For comparison, the jet images were taken at collector speeds of 1 × CTS, 2 × CTS, and 3 × CTS.

2.3 | The theory of measuring jet diameter

It is assumed that the cross-section for each jet segment along the spinline is circular. The jet diameter is defined as the length of the line perpendicular to the jet's medial axis and ends by the jet edges. Specifically, the jet diameter is achieved after four processing steps, that is, the edge detection, skeleton (medial axis) extraction, fitting, and calculation.

1. Since edge detection is sensitive to image noise, we use Gaussian denoising to reduce the noise first and then use Canny edge detection to extract the edges after changing the original image to a binary image (Figure 2A_ii).
2. The skeleton extraction is realized by the Zhang-Suen thinning algorithm. Since this algorithm uses an iteration to gradually delete the edge pixels, the jet in the binary image needs to fill in pixels (Figure 2A_iii).
3. The two processes mentioned above can achieve discrete data of the edges and the medial axis. Thus, it is necessary to smooth the discrete data to reduce the actual error after calculation. We apply polynomial equations to fit the curves, and the degree is set within 8–12 by trial and error (Figure 2A_iv).
4. The last step is calculating the jet diameter and the length of the medial axis (Figure 2A_v). The function of the normal of the medial axis (g_n) is

$$g_n(x) = -\frac{x}{f'_{\mathrm{mid}}(x_n)} + \frac{x_n}{f'_{\mathrm{mid}}(x_n)} + f_{\mathrm{mid}}(x_n), \quad (1)$$

where n is a positive integer, and $f_{\mathrm{mid}}(x)$ is the function of the medial axis. When the line of the g_n and the lines of $f_{\mathrm{left}}(x)$ and the $f_{\mathrm{right}}(x)$ (the functions of the left and the right jet profiles) intersect, we can achieve the abscissas $x = x_{\mathrm{left\_}n}$ and $x = x_{\mathrm{right\_}n}$. Then the function of jet diameter (d_n) can be expressed as

$$d_n = \sqrt{\left(x_{\mathrm{right\_}n} - x_{\mathrm{left\_}n}\right)^2 + \left(g_n\left(x_{\mathrm{right\_}n}\right) - g_n\left(x_{\mathrm{left\_}n}\right)\right)^2}. \quad (2)$$

The length of the medial axis can be written as

$$L(x) = \int_{x_0}^{x_n} \sqrt{1 + \left[f'_{\mathrm{mid}}(x)\right]^2}\, dx. \quad (3)$$

At last, the actual jet dimension should be transformed according to the outer diameter of the nozzle.

2.4 | The system interface diagram

Figure 2B displays the system interface diagram. After uploading a jet image, users can automatically achieve a plot of jet diameter along the spinline. The interface also contains the images after edge detection, skeleton extraction, fitting, and calculation. The source code for the application used here can be accessed from an open-source repository (https://github.com/whx-xyhf/visual-3D-printing) and is hosted online for simplified access. (http://124.220.224.64). Video S1 (Supporting Information) displays the operation of the software.

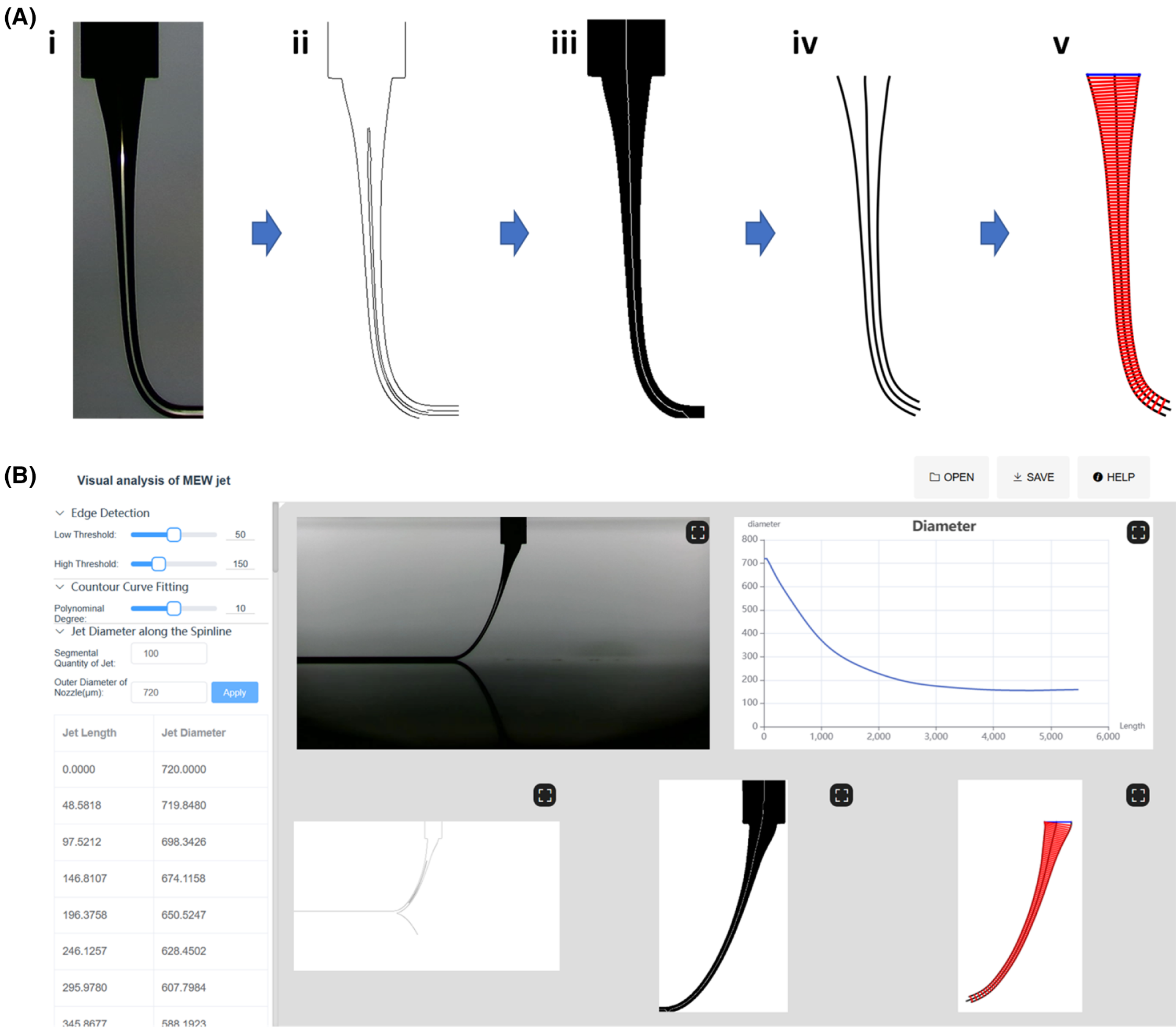

FIGURE 2 (A) A flow diagram of achieving jet diameters, including (i) uploading an original image, (ii) edge detection, (iii) skeleton (medial axis) extraction, (iv) fitting, and (v) calculation. (B) A screenshot of the website (http://124.220.224.64).

3 | RESULTS AND DISCUSSION

Digitally measuring the jet diameter reported here uses the same procedure as manually measuring the diameter.[12] Thus, it is meaningful to compare their differences. CTS is a crucial index in MEW to guide the suitable print. The print speed is generally set between $1 \times$ CTS and $3 \times$ CTS, so we compared the manually and digitally measured data for printing at $1 \times$ CTS, $2 \times$ CTS, and $3 \times$ CTS (Figure 3).

The jet length is close to the nozzle-to-collector distance at $1 \times$ CTS, and the jet length increases with increasing the print speed because of the drawing process. Overall, the digital data match the manual data for different print speeds. To analyze their differences quantitatively, we must compare the digitally and manually measured jet diameters at the same position. Instead of comparing the data of jet diameter processed from the fitting lines of the medial lines, comparing the data processed from the discrete point of the medial lines can reduce the error caused by fitting. Accordingly, the initial step is finding the same point along the spinline for the manually and digitally processed data. Herein the quadratic interpolation method was adopted. Table 1 lists the errors between the manual and the digital data. The length of the jet was divided into three regions; that is, the Taylor-cone region ($L \le 500$), the middle region ($500 < L \le 2500$), and the tail region ($L > 2500$). The Taylor-cone region can evaluate the print stability; the middle region contributes to the jet elongation; and the tail region influences the

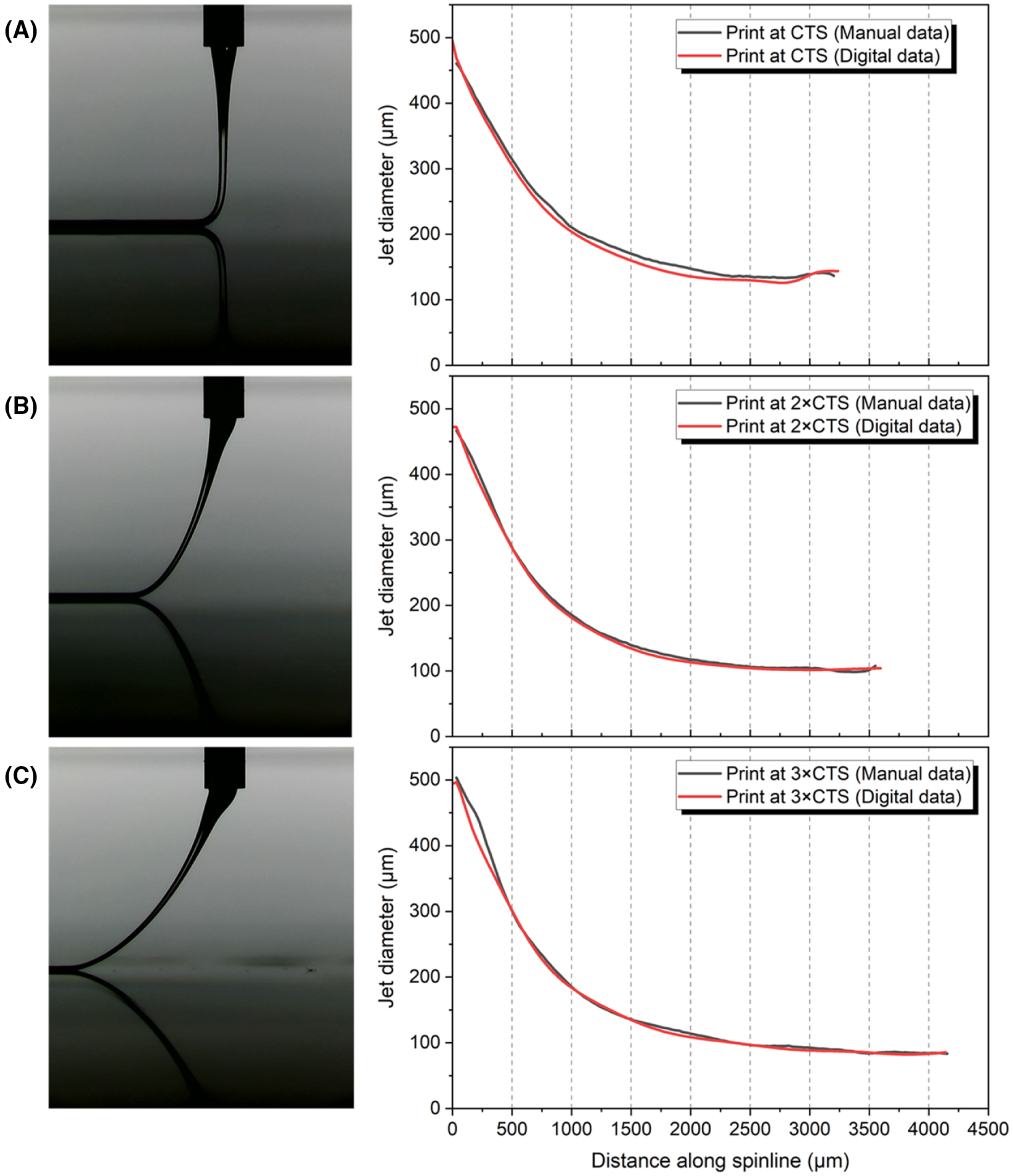

FIGURE 3 The manually and digitally measured jet diameter along the spinline. The jet is individually printed at (A) 1 × CTS, (B) 2 × CTS, and (C) 3 × CTS.

TABLE 1 Errors between the manually and the digitally processed data.

	Distance along the medial line (μm)	Mean absolute error (%)	Maximum error (%)	Minimum error (%)
1 × CTS	$L \leq 500$	1.91	1.72	−2.82
	$500 < L \leq 2500$	5.39	−3.02	−8.40
	$L > 2500$	3.72	5.44	−5.93
2 × CTS	$L \leq 500$	1.78	1.11	−3.32
	$500 < L \leq 2500$	2.79	−0.08	−4.73
	$L > 2500$	2.53	4.72	−3.62
3 × CTS	$L \leq 500$	4.20	0.02	−8.38
	$500 < L \leq 2500$	2.13	1.74	−5.62
	$L > 2500$	2.46	2.75	−5.28

proper overlay and adhesion of fiber layers. For each jet segment, the maximum error is less than 9%, indicating that the developed software can replace the manual processing of measuring each jet diameter.

4 | CONCLUSION

We successfully developed an accessible software enabling the measurement of jet diameter along its spinline. The digital processing is more efficient than the manual processing while can keep the data accurate. Meanwhile, we clarified the method of achieving clear jet images to enhance the quality of data extraction. It is a fundamental work of achieving basic jet data for further analysis of jet electrohydrodynamics.

ACKNOWLEDGMENTS

This work was supported by the National Natural Science Foundation of China (No. 62277013, No.62177040), National Statistical Science Research Project (No. 2023LZ035), Public Welfare Plan Research Project of Zhejiang Provincial Science and Technology Department (No. LTGG23H260003).

CONFLICT OF INTEREST STATEMENT

The authors declare that they have no conflicts of interest.

DATA AVAILABILITY STATEMENT

The data that support the findings of this study are available from the corresponding author upon reasonable request.

ORCID

Huaizhong Xu https://orcid.org/0000-0001-7291-1936

REFERENCES

1. Xu H, Du L. Sustainable medical materials printed by melt electrowriting: a mini-review. *Curr Opin Biomed Eng*. 2023;27:100464.
2. Wunner FM, Eggert S, Maartens J, et al. Design and development of a three-dimensional printing high-throughput melt Electrowriting technology platform. *3D Printing and Additive Manufacturing*. 2019;6(2):82-90.
3. McColl E, Groll J, Jungst T, Dalton PD. Design and fabrication of melt electrowritten tubes using intuitive software. *Mater Des*. 2018;155:46-58.
4. Eberle F, Gruska AK, Filippi B, et al. Hollow-fiber melt Electrowriting using a 3D-printed coaxial nozzle. *Adv Eng Mater*. 2021;24(1):2100750.
5. Xu H, Liashenko I, Lucchetti A, et al. Designing with circular arc toolpaths to increase the complexity of melt Electrowriting. *Adv Mater Technol*. 2022;7(10):2101676.
6. Hochleitner G, Youssef A, Hrynevich A, et al. Fibre pulsing during melt electrospinning writing. *BioNanoMat*. 2016;17(3–4):159-171.
7. Kim J, Bakirci E, O'Neill KL, Hrynevich A, Dalton PD. Fiber bridging during melt Electrowriting of poly(ε-Caprolactone) and the influence of fiber diameter and wall height. *Macromol Mater Eng*. 2021;306(3):2000685.
8. Liashenko I, Hrynevich A, Dalton PD. Designing outside the box: unlocking the geometric freedom of melt Electrowriting using microscale layer shifting. *Adv Mater*. 2020;32(28):2001874.
9. Robinson TM, Hutmacher DW, Dalton PD. The next frontier in melt electrospinning: taming the jet. *Adv Funct Mater*. 2019;29(44):1904664.
10. Wunner FM, Mieszczanek P, Bas O, et al. Printomics: the high-throughput analysis of printing parameters applied to melt electrowriting. *Biofabrication*. 2019;11(2):025004.
11. Mieszczanek P, Robinson TM, Dalton PD, Hutmacher DW. Convergence of machine vision and melt Electrowriting. *Adv Mater*. 2021;33(29):e2100519.
12. Ashour S, Xu H. Melt electrowriting: a study of jet diameters and jet speeds along the spinline. *Polym Adv Technol*. 2022;33(9):3013-3016.
13. Xu T, Gu J, Meng J, Du L, Kumar A, Xu H. Melt electrowriting reinforced composite membrane for controlled drug release. *J Mech Behav Biomed Mater*. 2022;132:105277.

SUPPORTING INFORMATION

Additional supporting information can be found online in the Supporting Information section at the end of this article.

How to cite this article: Zhou Z, Lu K, Wang H, et al. Development of an intuitive visualization system for measuring the melt electrowritten (MEW) jet diameter along the spinline. *Polym Adv Technol*. 2024;35(1):e6280. doi:10.1002/pat.6280